ADVANCED OPTICAL MATERIALS
www.advopticalmat.de

Dynamic Control of the Extraordinary Optical Scattering in Semicontinuous 2D Metamaterials

*Xiong Li, Mingbo Pu, Yanqin Wang, Xiaoliang Ma, Yang Li, Hui Gao, Zeyu Zhao, Ping Gao, Changtao Wang, and Xiangang Luo**

As one of the basis of traditional optics, Snell's law allows one to calculate the reflection and refraction angles for light passing from one medium to another.[1] For hundreds of years, it was thought that this law is a fundamental aspect of optics. After the pioneering work of Maxwell in 1865, the essence of Snell's law is now attributed to the continuity of electromagnetic boundary conditions. Although Snell's law is correct for ideal planar boundary between two normal materials, in the last several decades, it was shown that this law should be generalized to account for some abnormal properties of materials. As early as 1963,[2] Bloembergen and co-workers showed how to generalize this law to nonlinear material boundary, and how to calculate the reflection and refraction directions of harmonic light.

More recently, metasurface-assisted-Snell's law was also proposed to account for the additional momentum provided by the gradient surface structures.[3–6] In general, gradient metasurfaces are constructed by arrays of subwavelength scatters or apertures, which could generate local phase shift to an arbitrary wavefront. With these additional phases, the wavefront could be shaped on demand to construct many novel optical devices, such as beam deflectors,[3,4] focusing lenses,[7–9] spiral phase plates,[10] axicons,[7,11] hologram,[12,13] to name a few. It should be noted that similar phenomena by using reflectarrays or transmittarrays have also been demonstrated in the microwave regime, where metallic components are commonly used to control the phase retardation.[14–16]

Gradient metasurfaces based on Pancharatnam–Berry (PB) phase is a promising research area,[17] in which the phase shift depends on the geometry not the phase accumulation of propagation, enabling ultrathin profile and an integration into compact platforms. One common aspect of gradient metasurfaces based on PB phase scheme is that they rely on the polarization conversion process, either between linear polarizations[3,4] or circular polarizations.[8,13,18] Although it is very flexible in the tuning of phase shift, the polarization conversion efficiency of PB phase metasurfaces is normally not high enough for many applications. The value of efficiency for ultrathin single-layered metallic metasurface operating in transmission mode is typically in the order of a few percents.[3,4,7–9] Recently, it was demonstrated that the efficiency can reach 24.7% in the microwave region with a thickness of $1/1000\lambda$.[19] However, the theoretically predicted upper limit 25% is the intrinsic obstacle for its further improving.[20] In the last several years, it was demonstrated that coherent control could be used to dynamically change the light-matter interaction on the metasurface.[21–23] Electromagnetic wave could be completely absorbed by an ultrathin metasurface in an unexpected broad frequency range with coherent illumination,[23] which broke the classic bandwidth-thickness limit.[5] Besides, the polarization states could also be coherently controlled as demonstrated in previous work, and the efficiency could reach near 100% with frequency-independent property.[24,25] Very recently, spatial mode multiplexing by coherent control method is also reported.[26] Furthermore, the coherent control method provides a viable alternative for the signal processing based on nonlinear materials. Since nonlinear process is not needed anymore, the signal intensity as well as the thermal problems can be dramatically reduced.[21,27]

Here we show that nanoslit arrays with semicontinuous shape perforated in metallic screen could generate continuous phase distribution, thus altering the Snell's law in a more smooth way. A coherent control method is utilized to surpass the intrinsic efficiency limit of the metasurface in transmission mode and realize dynamic control over the generalized Snell's law. Our proof-of-concept experiment validates this method, providing a promising route to the practicality of a variety of devices based on metasurface structures.

In this paper, an ultrathin metallic metasurface with semicontinuous space-variant slit is used to generate perfect linear phase distribution, which has been demonstrated to have broader working bandwidth and higher efficiency compared to metasurfaces based on discrete metallic structures.[28] By defining ξ as the angle between the slit and the x-axis as shown in Figure S1 (Supporting Information) and recalling that $\Phi = 2\sigma\zeta$ is the PB phase (see Supporting Information), the tangent $d\gamma/dx = \sigma\tan(k_a x/2)$ can be directly integrated over the x-axis to obtain the analytic curve as follows

$$\gamma = -\frac{2\sigma}{k_a}\ln\left(\left|\cos(k_a x/2)\right|\right) \quad (1)$$

where k_a is the additional horizontal wavevector of the generated beam, $\sigma = \pm 1$ denotes the left and right handed circular polarization (LCP and RCP).

Since different circular polarization only introduce a reverse of the sign, we chose $\sigma = 1$ in the following discussion.

Dr. X. Li, Dr. M. Pu, Dr. Y. Wang, Dr. X. Ma, Dr. Y. Li, Dr. H. Gao, Prof. Z. Zhao, Dr. P. Gao, Prof. C. Wang, Prof. X. Luo
State Key Laboratory of Optical Technologies on Nano-Fabrication and Micro-Engineering
Institute of Optics and Electronics
Chinese Academy of Sciences
Chengdu 610209, China
E-mail: lxg@ioe.ac.cn

DOI: 10.1002/adom.201500713

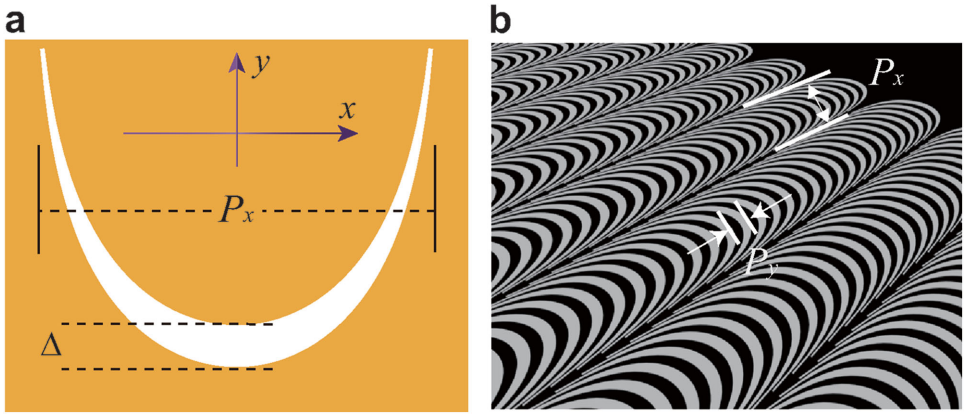

Figure 1. Catenary aperture and its application in optical metasurfaces. a) Schematic of the catenary aperture. b) Sketch of the catenary array.

Interestingly, Equation (1) is just the catenary equation normally exists in suspension bridges.[29] By shifting this curve with Δ along y direction, a catenary-shaped slit can be formed as shown in **Figure 1**a. The value of Δ should be much smaller than the working wavelength in order to eliminate the effect of high order electromagnetic modes in the catenary apertures. Subsequently, the catenary apertures are arranged in a linear array with a period of P_x = 2 μm and $P_y = 2\Delta$ = 400 nm along the x direction and y direction, respectively, shown in Figure 1b. Because the value of Equation (1) is infinite for $x = \pm P_x/2 + mP_x$ (m is an integer), so we truncated the curves at the two ends with $\Delta x = P_x/20$ in practical designs. After the truncation, the four tips of the two catenary curves are connected to obtain the catenary aperture.[28]

A sample was fabricated by focus ion beam (FIB) milling in a 120-nm-thick gold layer, which is deposited on quartz substrate. The inset of **Figure 2** shows the scanning electron microscopy (SEM) image of the fabricated sample. The abnormal deflection of the beam deflector was measured, as shown in Figure S2 (Supporting Information). The deflection angle agrees well with our expectation in a broadband wavelength range (see the Supporting Information for details). In order to characterize the efficiency of both the abnormal transmission and reflection, the ratio of the deflected power to the input power was measured, as shown in Figure 2. The theoretical values were evaluated by using the method we introduced previously,[28] while setting the grating period to 300 nm. The efficiency is much higher than that of the single-layered metasurfaces based on discrete metallic scatters or apertures.[3,4,7–9] The relatively large deviation of the transmittance data between the calculations and the experiments is possibly attributed to the multireflections in the substrate and the fabrication errors.

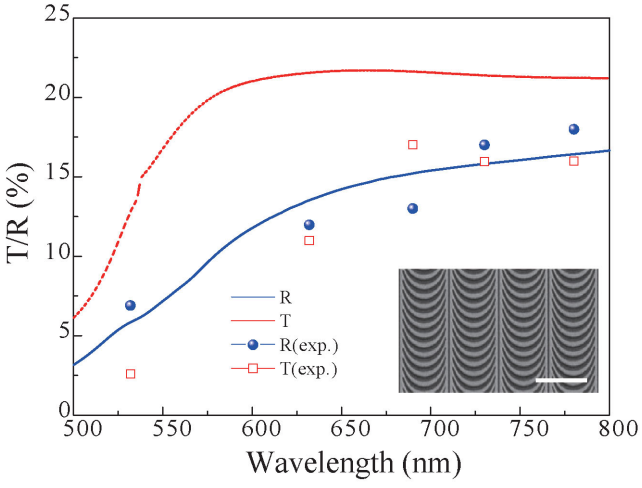

Figure 2. Theoretical and experimental transmittance and reflectance for the cross-polarization. Inset shows the scanning electron microscopy (SEM) image of the sample. Scale bar, 2 μm.

As discussed above, the efficiency of a single-layered ultrathin metasurface is theoretically limited. In the following, we show that the efficiency of this kind of metasurface can be boosted with the concepts borrowed from the "coherent perfect absorber" or "antilaser".[23,30,31] Owing to the coupling of the reflection and transmission, two counter-propagating beams could interact strongly in the metasurface, leading to coherently enhancing or decreasing the abnormal deflection effect.

In our implementation, two collimated counterpropagating laser beams (the signal and control beams) in freespace are directed onto opposite surfaces of the sample, as illustrated in **Figure 3**. Before illuminated on the sample, the two beams are converted to be right-circularly polarized (RCP) and left-circularly polarized (LCP), respectively, through cascaded polarizer and quarter-waveplate. Assuming that the amplitude of the two beams is 1 and s, and the reflection and transmission amplitudes are equal, the electric fields in the right side of the sample can be written as (see the Supporting Information for details)

$$\begin{aligned}\begin{bmatrix} E_x \\ E_y \end{bmatrix} &= \begin{bmatrix} E_{tx} \\ E_{ty} \end{bmatrix} + s\begin{bmatrix} E_{rx} \\ E_{ry} \end{bmatrix} \\ &= \left\{(t_u + t_v)\begin{bmatrix} 1 \\ i\sigma \end{bmatrix} + (t_u - t_v)e^{2i\sigma\zeta}\begin{bmatrix} 1 \\ -i\sigma \end{bmatrix}\right\} \\ &\quad + s\left\{(r_u + r_v)\begin{bmatrix} 1 \\ i\sigma \end{bmatrix} + (r_u - r_v)e^{2i\sigma\zeta}\begin{bmatrix} 1 \\ -i\sigma \end{bmatrix}\right\} \\ &= \left\{(t_u + t_v) + s(r_u + r_v)\right\}\begin{bmatrix} 1 \\ i\sigma \end{bmatrix} \\ &\quad + \left\{(t_u - t_v) + s(r_u - r_v)\right\}e^{2i\sigma\zeta}\begin{bmatrix} 1 \\ -i\sigma \end{bmatrix}\end{aligned} \tag{2}$$

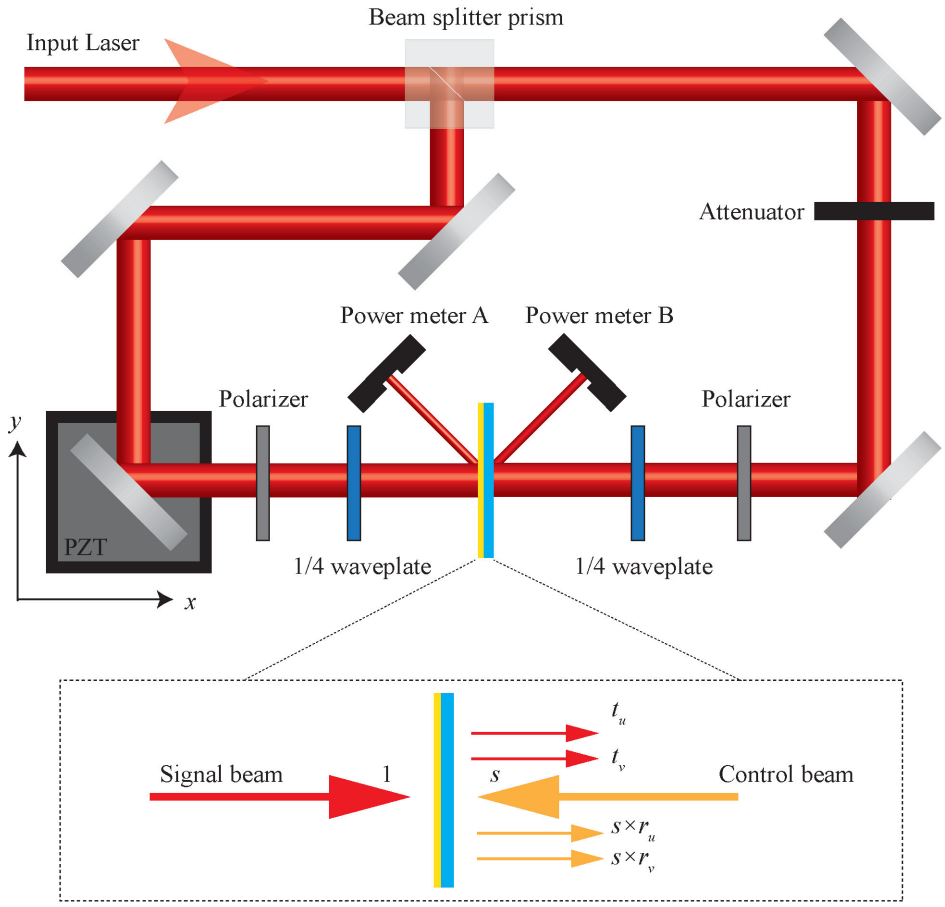

Figure 3. Experimental configuration. Laser beams from a diode-pumped solid-state laser (532 nm) and He–Ne laser (632.8 nm) enter a beam splitter (BS). The two split beams are directed normally onto opposite sides of our sample. A phase delay in one of the beam paths controls the relative phase difference between the two beams, by moving a piezo-actuated nanopositioning stage with 0.8 nm resolution (P-612.2SL, Physik Instrumente (PI) GmbH & Co. KG). An additional attenuator ensures that the transmitted beams have equal intensities, compensating for imbalances in the beam splitters and the inherent asymmetry of our sample. The two abnormal output beams, which are the superposition of abnormal transmitted beam and abnormal reflected beam, are collected by two power meters synchronously. The inset is a schematic of the dynamic control of metasurface.

where r and t denote the complex reflection and transmission coefficients, u and v represent the local coordinates of the anisotropic elements.

The output intensity of the cross-polarized component can be written as

$$I_{\text{cross}} = \left|(t_u - t_v) + S(r_u - r_v)\right|^2. \tag{3}$$

Obviously, I_{cross} is dependent on s, thus can be dynamically tuned by the control beam. The modulation depth, defined as the ratio of the maximum to the minimum intensity, is then

$$M = \frac{\max\left(\left|(t_u - t_v) + S(r_u - r_v)\right|^2\right)}{\min\left(\left|(t_u - t_v) + S(r_u - r_v)\right|^2\right)} \tag{4}$$

For ideal anisotropic structure, the transmission and reflection coefficients can be approximated as $t_u = 0$, $t_v = 1$, $r_u = -1$, and $r_v = 0$. In this case, the modulation depth can approach infinite since there is $I_{\text{cross}} = 0$ for $s = -1$.

We experimentally measured the intensity of the anomalous refraction and reflection with respect to the movement of the piezo-actuated nanopositioning stage corresponding to the phase difference between the two coherent light beams, as shown in **Figure 4**. In order to test the modulation ability and the efficiency enhancement of this method, we also observed the refracted and reflected power of single signal beam and control beam with respect to the movement of the nanopositioning stage for reference. The total refraction (T_{total}) is defined as the summation of the refraction of the signal beam and the reflection of the control beam. Similarly, the total reflection (R_{total}) is defined as the summation of the reflection of the signal beam and the refraction of the control beam.

First, we used a diode-pumped solid-state laser at $\lambda = 532$ nm as the laser source of coherent control. For single beam illumination, the values of both T_{total} and R_{total} nearly keep constant as the stage moving. When coherent illumination was adopted, a sinusoidal function type of intensity with respect to the movement was obtained through the phase difference control, as illustrated in Figure 4a. The position where the constructive interference occurs between the anomalous refracted

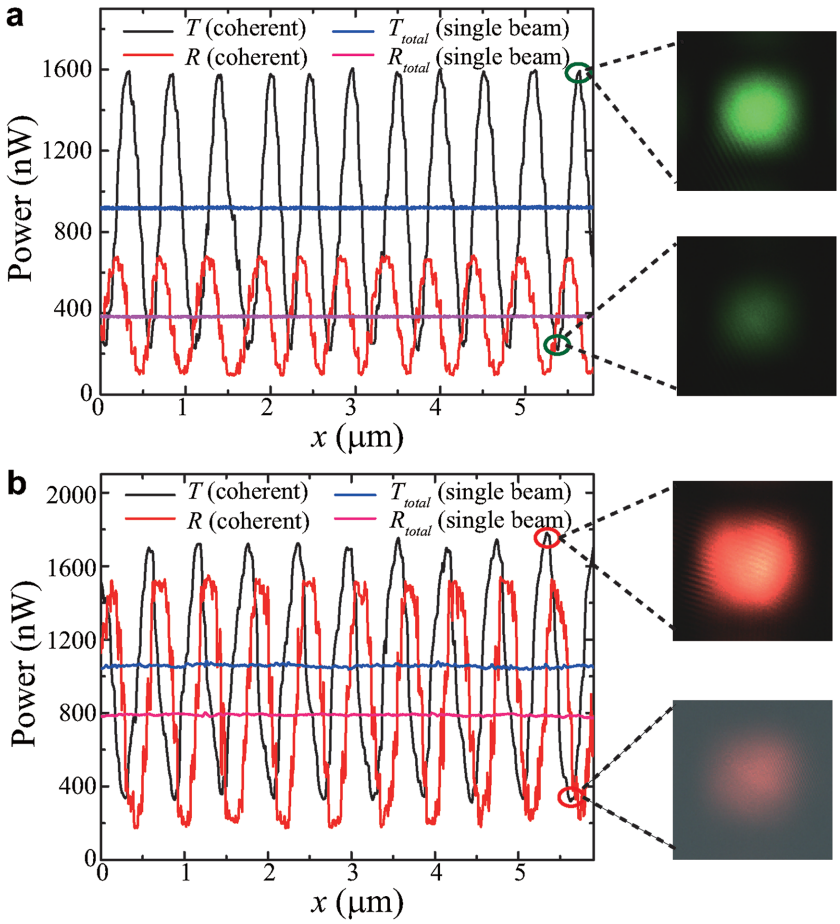

Figure 4. Abnormal transmission and reflection. Measured results of the abnormal transmission and reflection at a) $\lambda = 532$ nm and b) $\lambda = 632$ nm. The refraction spots in the insert were capture at 20 cm away from the output plane of the sample. The modulation depth in refraction at $\lambda = 532$ and 632 nm is 8:1 and 5.8:1, respectively.

beam of the signal light and the anomalous reflected beam of the control light corresponds to the peak of the sinusoidal function. Similarly, the destructive interference occurs at the position of the valley of the sinusoidal function. The average output power of coherent anomalous refracted beams and the anomalous reflected beams of signal light at the peaks is 78% and 62% enhanced, compared to that with no coherent illumination (T_{total} and R_{total}) as depicted in Figure 4a. The modulation of intensity is dynamic with the movement of stage, and the average period of the intensity modulation from experiment is 531.4 nm, matching well with the theoretical value 532 nm (wavelength of the incident light). The insert in Figure 4a plots the anomalous refracted spots at the marked peak and valley by a color CCD camera, showing good contrast. The experimental modulation depth of the sample is ≈8:1 at $\lambda = 532$ nm. The finite value of modulation depth is mainly attributed to the asymmetry of our sample due to the substrate.

In order to demonstrate that the coherent control method can enhance the efficiency in a broadband for our sample, a He-Ne laser with $\lambda = 632.8$ nm was also adopted in the coherent control experiment. Similar results were obtained as shown in Figure 4b. The average output power of coherent anomalous refracted beams and the anomalous reflected beams of signal light at the peaks is 62% and 88% enhanced respectively, compared to that with no coherent illumination.

To conclude, our theoretical and experimental results demonstrate unambiguously that the catenary slit array can be used to realize continuous phase control in the microscopic scale. The dynamic control over the anomalous reflection/transmission is theoretically analyzed and experimentally demonstrated. Our proof-of principle experiments indicate that the coherent control method can surpass the theoretical efficiency limit of metasurface. It should be noted that the application of this method is not limited to improve the efficiency of anomalous reflection/transmission beams which is demonstrated in this paper, but also a variety of other metasurface-based devices working in transmission mode, ranging from high efficiency metasurface lens, OAM generator to hologram. Our method may pave the way for the real-world applications of metasurface based ultrathin optical devices.

Experimental Section

All the samples are milled in an Au film on quartz substrate using a focused ion beam (FIB, FEI Helios Nanolab 650). To improve the adhesion between the Au film and the substrate, a 3-nm-thick Cr film and 120-nm-thick Au film are orderly deposited on a 1-mm-thick quartz substrate by magnetron sputtering.

Supporting Information

Supporting Information is available from the Wiley Online Library or from the author.

Acknowledgements

X.L., M.P., and Y.W. contributed equally to this work. The authors acknowledge the financial support by 973 Program of China under Contract No. 2013CBA01700 and National Natural Science Funds under Contact Nos. 61138002 and 61307043.

Received: December 2, 2015
Revised: December 30, 2015
Published online: January 28, 2016

[1] M. Born, E. Wolf, *Principle of Optics*, 7nd ed., Pergamon, Oxford, UK **2007**.
[2] J. Ducuing, N. Bloembergen, *Phys. Rev. Lett.* **1963**, *10*, 474.
[3] N. Yu, P. Genevet, M. A. Kats, F. Aieta, J.-P. Tetienne, F. Capasso, Z. Gaburro, *Science* **2011**, *334*, 333.

[4] X. Ni, N. K. Emani, A. V. Kildishev, A. Boltasseva, V. M. Shalaev, *Science* **2011**, *335*, 427.
[5] X. Luo, *Sci. China Phys. Mech. Astron.* **2015**, *58*, 594201.
[6] X. Luo, M. Pu, X. Ma, X. Li, *Int. J. Antennas Propag.* **2015**, *2015*, 204127.
[7] F. Aieta, P. Genevet, M. A. Kats, N. Yu, R. Blanchard, Z. Gaburro, F. Capasso, *Nano Lett.* **2012**, *12*, 4932.
[8] X. Chen, L. Huang, H. Mühlenbernd, G. Li, B. Bai, Q. Tan, G. Jin, C.-W. Qiu, S. Zhang, T. Zentgraf, *Nat. Commun.* **2012**, *3*, 1198.
[9] X. Ni, S. Ishii, A. V. Kildishev, V. M. Shalaev, *Light Sci. Appl.* **2013**, *2*, e72.
[10] P. Genevet, N. Yu, F. Aieta, J. Lin, M. A. Kats, R. Blanchard, M. O. Scully, Z. Gaburro, F. Capasso, *Appl. Phys. Lett.* **2012**, *100*, 013101.
[11] D. Lin, P. Fan, E. Hasman, M. L. Brongersma, *Science* **2014**, *345*, 298.
[12] W. T. Chen, K.-Y. Yang, C.-M. Wang, Y.-W. Huang, G. Sun, I. D. Chiang, C. Y. Liao, W.-L. Hsu, H. T. Lin, S. Sun, L. Zhou, A. Q. Liu, D. P. Tsai, *Nano Lett.* **2013**, *14*, 225.
[13] L. Huang, X. Chen, H. Mühlenbernd, H. Zhang, S. Chen, B. Bai, Q. Tan, G. Jin, K.-W. Cheah, C.-W. Qiu, J. Li, T. Zentgraf, S. Zhang, *Nat. Commun.* **2013**, *4*, 2808.
[14] J. Huang, J. A. Encinar, *Reflectarray Antennas*, John Wiley & Sons, Hoboken, NJ **2008**.
[15] S. V. Hum, J. Perruisseau-Carrier, *IEEE Trans. Antennas Propag.* **2014**, *62*, 183.
[16] X. Ma, W. Pan, C. Huang, M. Pu, Y. Wang, B. Zhao, J. Cui, C. Wang, X. Luo, *Adv. Opt. Mater.* **2014**, *2*, 945.
[17] Z. Bomzon, G. Biener, V. Kleiner, E. Hasman, *Opt. Lett.* **2002**, *27*, 1141.
[18] X. Ma, M. Pu, X. Li, C. Huang, Y. Wang, W. Pan, B. Zhao, J. Cui, C. Wang, Z. Zhao, X. Luo, *Sci. Rep.* **2015**, *5*, 10365.
[19] X. Ding, F. Monticone, K. Zhang, L. Zhang, D. Gao, S. N. Burokur, A. de Lustrac, Q. Wu, C.-W. Qiu, A. Alù, *Adv. Mater.* **2015**, *27*, 1195.
[20] F. Monticone, N. M. Estakhri, A. Alù, *Phys. Rev. Lett.* **2013**, *110*, 203903.
[21] J. Zhang, K. F. MacDonald, N. I. Zheludev, *Light Sci. Appl.* **2012**, *1*, e18.
[22] J. Shi, X. Fang, E. T. F. Rogers, E. Plum, K. F. MacDonald, N. I. Zheludev, *Opt. Express* **2014**, *22*, 21051.
[23] M. Pu, Q. Feng, M. Wang, C. Hu, C. Huang, X. Ma, Z. Zhao, C. Wang, X. Luo, *Opt. Express* **2012**, *20*, 2246.
[24] M. Crescimanno, N. J. Dawson, J. H. Andrews, *Phys. Rev. A* **2012**, *86*, 031807.
[25] Y. Wang, M. Pu, C. Hu, Z. Zhao, C. Wang, X. Luo, *Opt. Commun.* **2014**, *319*, 14.
[26] M. Papaioannou, E. Plum, J. Valente, E. T. F. Rogers, N. I. Zheludev, *presented at CLEO_Europe*, Munich, Germany, June **2015**.
[27] X. Fang, K. F. MacDonald, N. I. Zheludev, *Light Sci. Appl.* **2015**, *4*, e292.
[28] M. Pu, X. Li, X. Ma, Y. Wang, Z. Zhao, C. Wang, C. Hu, P. Gao, C. Huang, H. Ren, X. Li, F. Qin, J. Yang, M. Gu, M. Hong, X. Luo, *Sci. Adv.* **2015**, *1*, e1500396.
[29] D. Gilbert, *Philos. Trans. R. Soc. London* **1826**, *116*, 202.
[30] Y. D. Chong, L. Ge, H. Cao, A. D. Stone, *Phys. Rev. Lett.* **2010**, *105*, 053901.
[31] W. Wan, Y. Chong, L. Ge, H. Noh, A. D. Stone, H. Cao, *Science* **2011**, *331*, 889.